**SUPPLEMENTARY MATERIALS**
**for**
# Mapping the structural and functional network architecture of the medial temporal lobe using 7T MRI

Preya Shah[1,2], Danielle S. Bassett[1,3], Laura E.M. Wisse[4,5], John A. Detre[5,6,7], Joel M. Stein[5], Paul A. Yushkevich[4,5], Russell T. Shinohara[8], John B. Pluta[4,5], Elijah Valenciano[4], Molly Daffner[6,9], David A. Wolk[6,9], Mark A. Elliott[5], Brian Litt[1,2,6], Kathryn A. Davis[2,6,§], Sandhitsu R. Das[4,5,§]

1. Department of Bioengineering, University of Pennsylvania, Philadelphia, PA, 19104, USA
2. Center for Neuroengineering and Therapeutics, University of Pennsylvania, Philadelphia, PA, USA
3. Department of Electrical & Systems Engineering, University of Pennsylvania, Philadelphia, PA, USA
4. Penn Image Computing and Science Laboratory, University of Pennsylvania, Philadelphia, PA, USA
5. Department of Radiology, University of Pennsylvania, Philadelphia, PA, USA
6. Department of Neurology, University of Pennsylvania, Philadelphia, PA, USA
7. Center for Functional Neuroimaging, University of Pennsylvania, Philadelphia, PA, USA
8. Department of Biostatistics, Epidemiology, and Informatics, University of Pennsylvania, Philadelphia, PA, USA
9. Penn Memory Center, University of Pennsylvania, Philadelphia, PA, USA
§ Both authors contributed equally to this work

Corresponding author: Preya Shah (preya@pennmedicine.upenn.edu)
Institution: University of Pennsylvania

Short title: Mapping MTL subregional connectivity networks
**Keywords:** hippocampus, subfields, 7 tesla, image segmentation, resting state fMRI, network neuroscience

**Supplementary Material Contents:**



## S1. Supplemental Analysis:

*S1.1: Binary Network Analysis*

We chose to utilize weighted networks for our primary analysis, as there is evidence that connection strength carries important information about network architecture [Bassett and Bullmore, 2016] and that weak connections show potential as disease biomarkers [Bassett et al., 2012]. Though weighted networks may provide richer information, a vast amount of prior and current literature utilizes networks which are binarized using a fixed threshold and then analyzed using various graph-theoretical metrics. With that in mind, we repeated our analysis using binary graphs to facilitate interpretability and applicability of our findings to those of other brain connectivity studies. All code for this analysis is also included in our publicly available repository at https://github.com/shahpreya/MTLnet.

We generated a series of binary networks by thresholding our group-level networks across a range of densities, in 5% increments, in order to retain 1%–50% of all possible edges in the network [Achard and Bullmore, 2007]. For each density, we computed network degree, clustering coefficient, and local efficiency using the commonly accepted binary definitions of these metrics [Rubinov and Sporns 2010]. We computed subregion-level asymmetry indices ([R-L)]/[R+L]) for these metrics, as well as overall network asymmetry. Bootstrapping (sampling subjects with replacement) was used to assess variability of these network metrics. We determined the significance of network asymmetries by permuting the nodes (i.e subregions) of the generated networks (1000 iterations) and generating a null distribution of network asymmetries. Modular organization and modular significance was computed using the same

methods as those for the weighted networks. Finally, in order to evaluate the relationship between structural and functional connectivity, we computed the Dice Similarity Coefficient (DSC) to quantify the overlap between the structural and functional adjacency matrices for each density value. The significance of these DSCs was determined by generating a null distribution of DSCs by permuting the edges of the network (1000 iterations).

We found that binary networks exhibited significantly strong symmetry ($p<0.05$) across all density ranges for functional networks (**Supp. Figure 4.1**), and for densities less than 25% for the structural networks (**Supp. Figure 4.2**). Moreover, we determined that the modular organization at fixed density thresholds was similar to that observed in the weighted networks, with a strong degree of interhemispheric connectivity and a segregation of hippocampal and extrahippocampal structures. Finally, the level of overlap between structural and functional networks was significant for most densities up to 30% (**Supp. Figure 4.3**). While we believe that binary networks are not as robust and representative of underlying physiology as weighted networks, it is still reassuring that our broad conclusions hold up when carrying out analysis on binary networks.

**S2: Supplementary Figures**

| | Computed Volumes ($mm^3$) | | Reference Volumes ($mm^3$) | |
|---|---|---|---|---|
| | **Left** | **Right** | **Histology** | **Imaging** |
| **CA1** | 821 ± 182 | 804 ± 160 | 591[3], 641[4] | 1420-L*, 1530-R*, 520[2] |
| **CA2** | 26.2 ± 8.70 | 30.4 ± 11.3 | see CA3 | 60-L*, 71-R*, see CA3 |
| **CA3** | 107 ± 19 | 88.9 ± 26.3 | 139[3], 138[4] (CA2+3) | 120* (CA3), 179[2] (CA2+3) |
| **DG** | 623 ± 123 | 740 ± 128 | 256[3], 219[4] | 790-L*, 800-R*, 455[2] |
| **Tail** | 315 ± 83.0 | 296 ± 69.9 | N/A | 465[2] |
| **Sub** | 837 ± 93.3 | 853 ± 97.7 | 404[3], 850[4] | 610-L*, 650-R*, 857[2] |
| **ERC** | 612 ± 85.4 | 588 ± 81.5 | N/A | 520-L*, 530-R* |
| **BA35** | 660 ± 90.0 | 608 ± 110 | N/A | see BA36 |
| **BA36** | 1816 ± 292 | 1646 ± 235 | N/A | 2585-L[1], 2577-R[1] (BA35+36) |
| **PHC** | 1093 ± 225 | 1047 ± 271 | N/A | 2675-L[5], 2469-R[5] |

**Supp. Table 1**: Computed MTL volumes and correspondence with reference volumes from prior histological and neuroimaging studies. *[Wisse et al., 2016], 1. [Insausti et al., 1998], 2. [Iglesias et al., 2015], 3. [Simic et al., 1997], 4. [Harding et al., 1998], 5. [Pruessner et al., 2002]

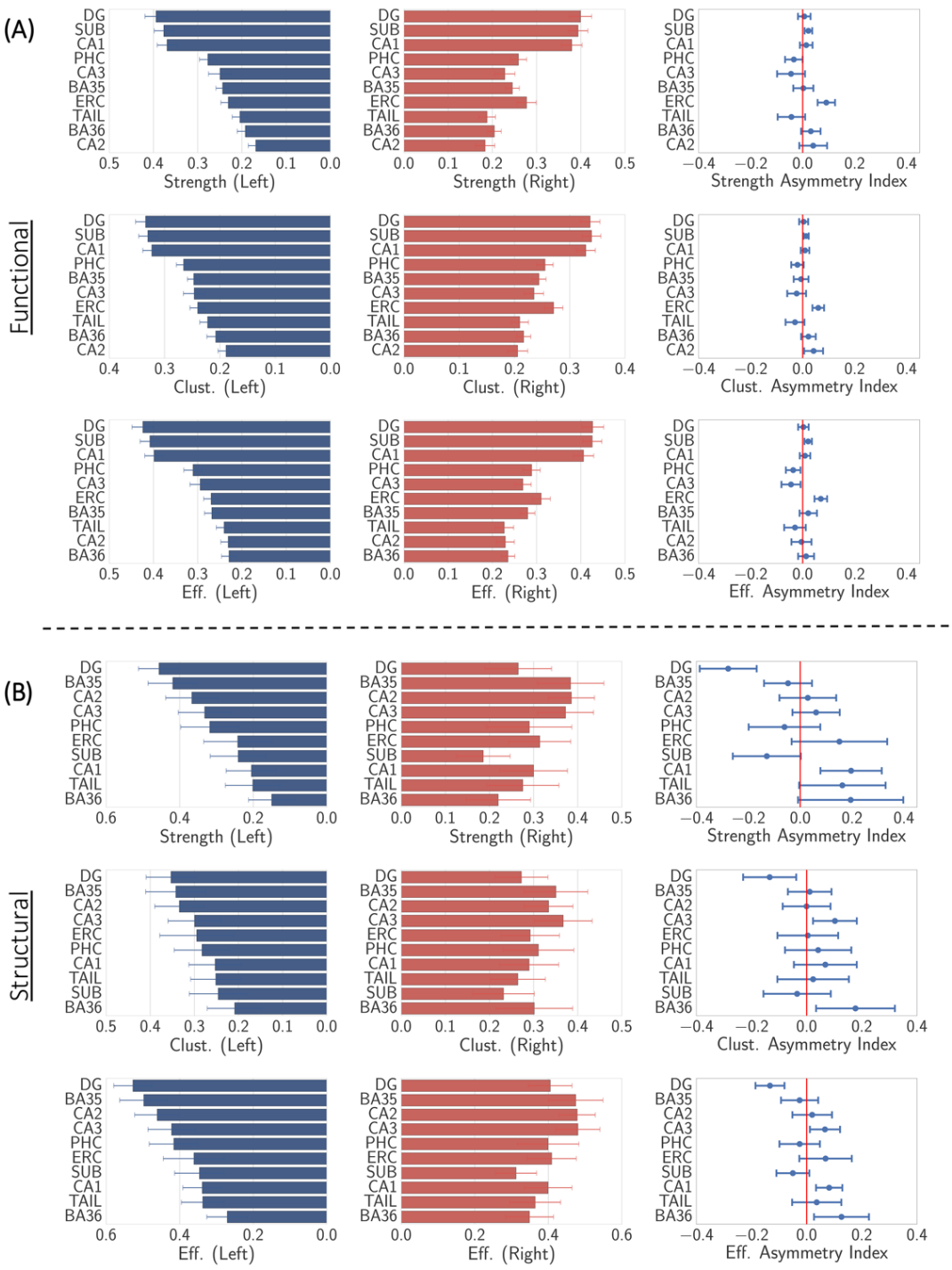


**Supp. Figure 1**: Functional (A) and structural (B) local network metrics (connectivity strength, clustering coefficient, and local efficiency) computed on bootstrapped matrices for left and right hemispheres (mean +/- S.D.), as well as corresponding asymmetry indices (mean +/- S.D.). For each plot, MTL subregions are rank-ordered based on network metric value for left hemisphere, in order to emphasize hubness of each subregion.

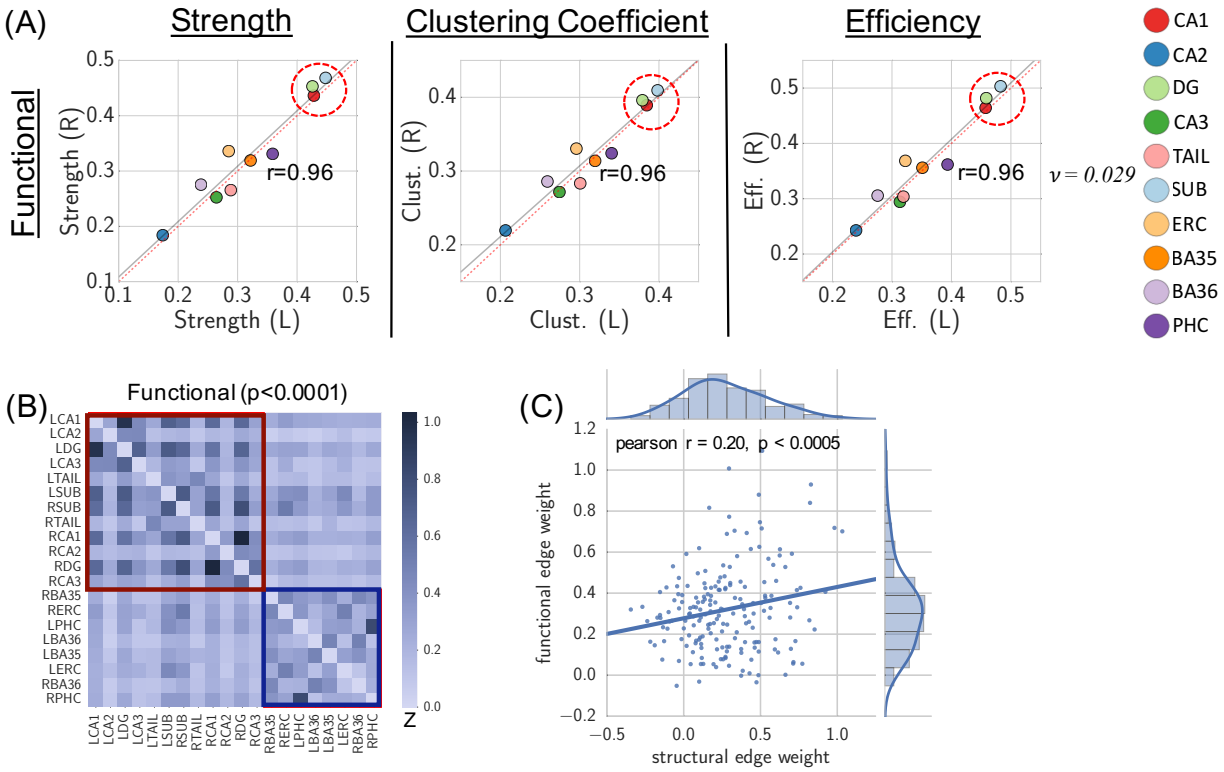


**Supp. Figure 2**: Functional network findings on images with no global signal regression: (A) functional symmetry across node-level metrics, (B) modular organization, and (C) structure-function correlation. We find significant functional symmetry ($\nu = 0.029$), significant modular organization identical to our original analysis, and significant structure function correlation (r=0.20), revealing that our findings are robust to the choice of global signal regression.

(A)

| Subregion | L Vol Mean | L Vol SD | R Vol Mean | R Vol SD |
|---|---|---|---|---|
| CA1 | 846.8 | 174.6 | 800.5 | 160.1 |
| CA2 | 24.78 | 6.893 | 29.09 | 11.08 |
| CA3 | 109.6 | 21.49 | 86.97 | 25.08 |
| DG | 574.5 | 89.84 | 735.2 | 118.6 |
| TAIL | 322 | 80.42 | 295.2 | 64.16 |
| SUB | 830.5 | 92.05 | 866 | 94.16 |
| ERC | 605.3 | 76.48 | 601.6 | 77.89 |
| BA35 | 650 | 80.17 | 591.3 | 111.1 |
| BA36 | 1843 | 269.2 | 1669 | 223.2 |
| PHC | 1126 | 207.4 | 1060 | 258.5 |
| HIPP | 2708 | 337.4 | 2813 | 338 |
| MTL | 6932 | 730.1 | 6735 | 661.8 |

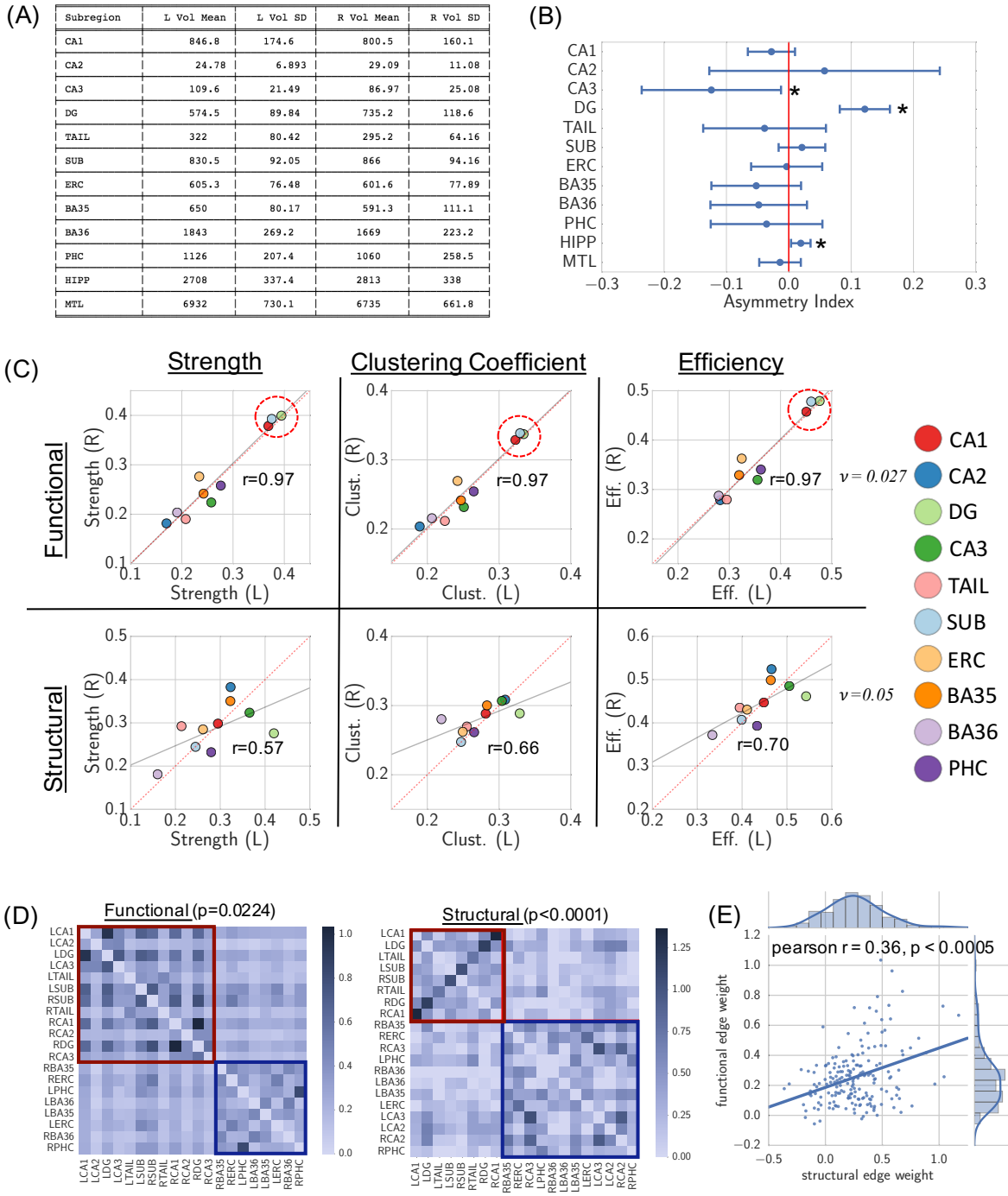


**Supp. Figure 3**: Structural and functional analyses replicated after replacing manual segmentations with corresponding automated segmentations: (A) subregion volumes, (B) subregional volumetric symmetry, (C) network symmetry, (D) modular organization, and (E) structure-function correlation. Similar to our primary analysis, we find significant volumetric asymmetry in DG, CA3, and hippocampus. Also, we find significant functional symmetry ($\nu = 0.029$), structural symmetry ($\nu = 0.05$), significant functional and structural modular organization identical to our original analysis, and significant structure function correlation (r=0.36), revealing that our findings are robust to the choice of segmentation approach

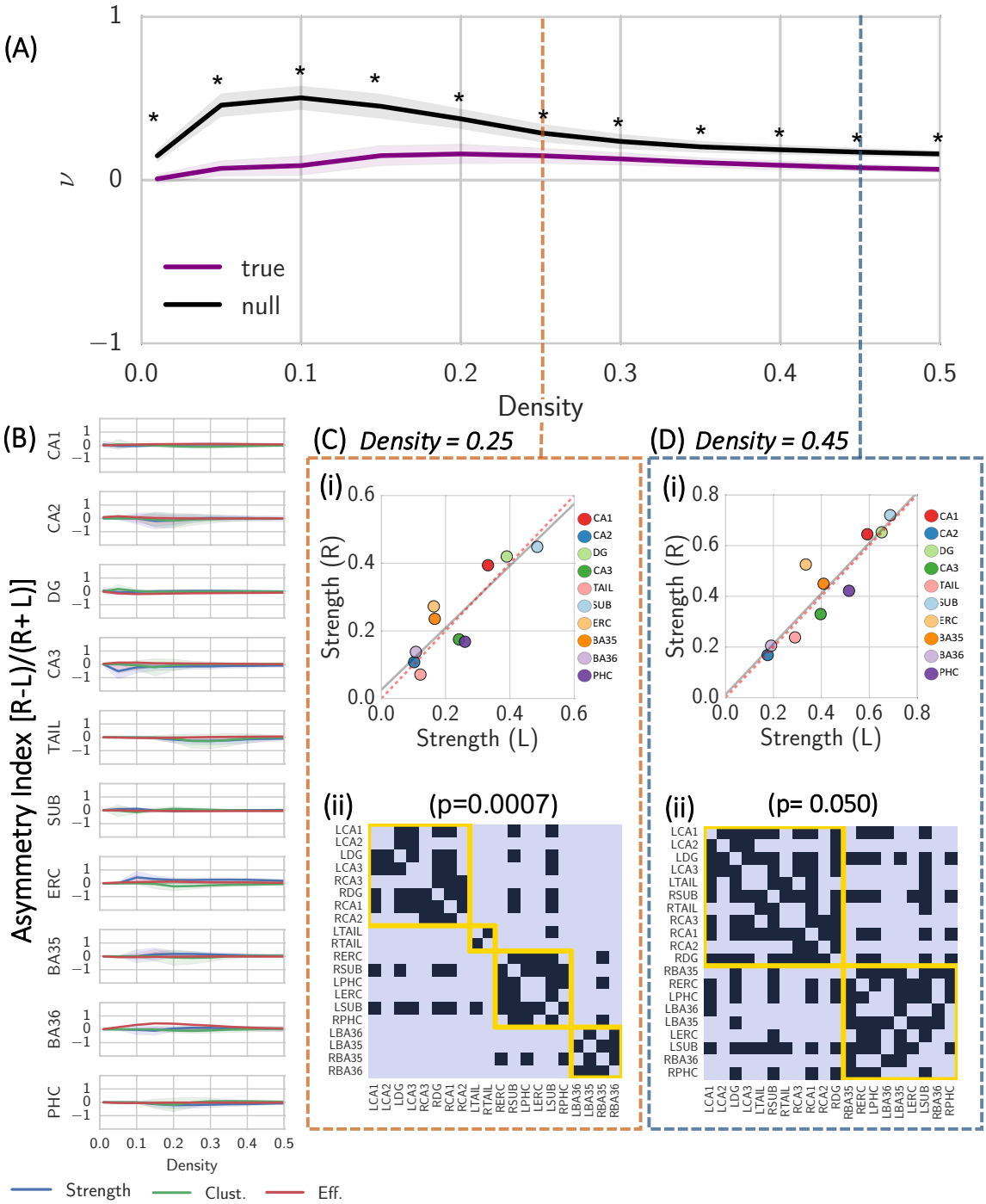


**Supp. Figure 4.1**: Functional binary network findings: (A) Network asymmetry across 1%-50% density range compared with null network asymmetry, significant across entire density range (*p < 0.05). (B) subregion level asymmetry indices for connectivity strength, clustering coefficient, and local efficiency. Envelopes represent standard deviation. For two example densities of (C) 25% and (D) 45%, we report (i) left-right correlation in connectivity strength and (ii) modular organization. We find a strong degree of functional symmetry, as well as significant modular organization which emphasizes strong interhemispheric connectivity and a hippocampal-parahippocampal delineation.

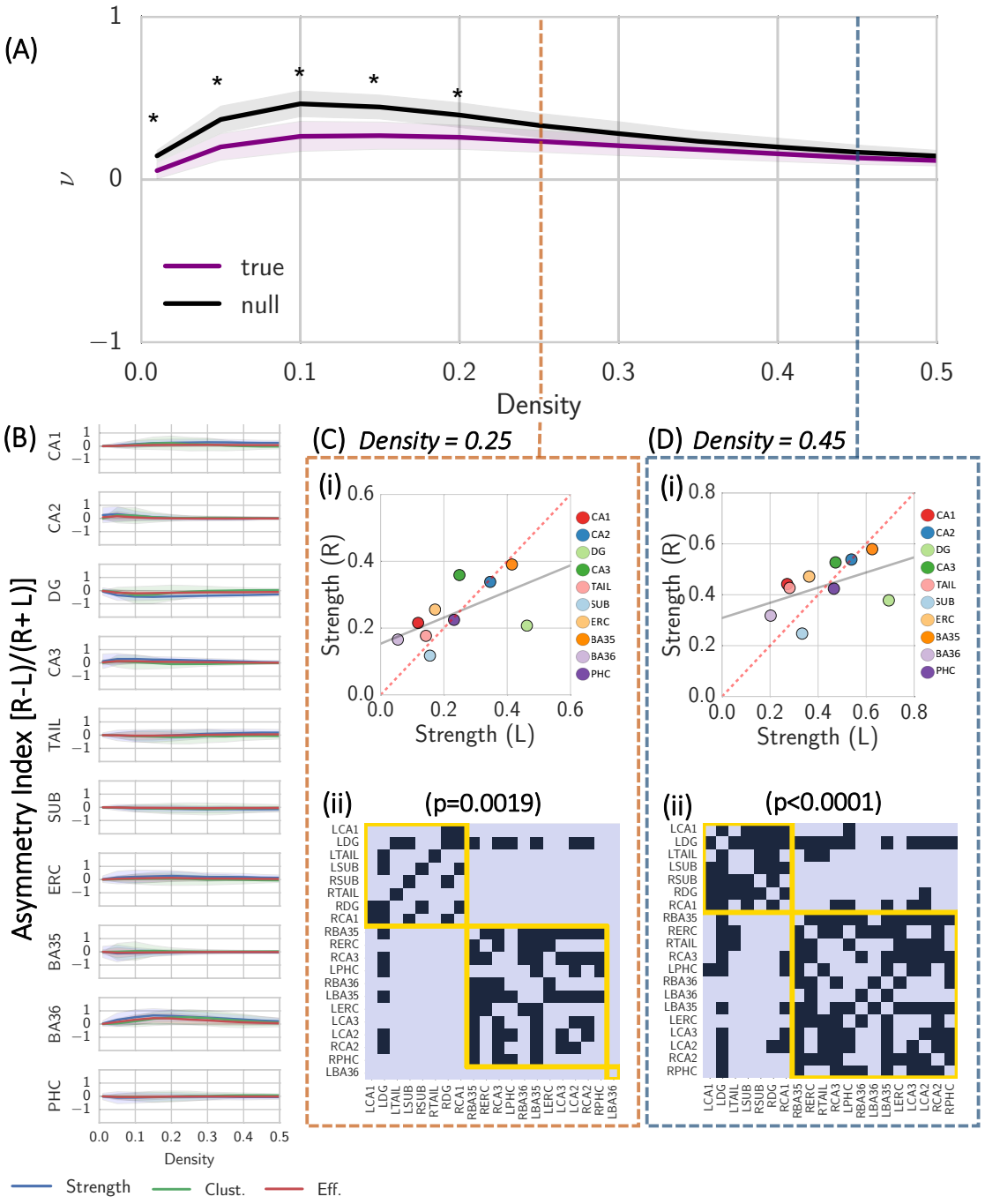


**Supp. Figure 4.2**: Structural binary network findings: (A) Network asymmetry across 1%-50% density range compared with null network asymmetry, significant across densities less than 25% (*p < 0.05). (B) subregion level asymmetry indices for connectivity strength, clustering coefficient, and local efficiency. Envelopes represent standard deviation. For two example densities of (C) 25% and (D) 45%, we report (i) left-right correlation in connectivity strength and (ii) modular organization. We find a strong degree of structural symmetry, as well as significant modular organization which emphasizes strong interhemispheric connectivity and a hippocampal-parahippocampal delineation.

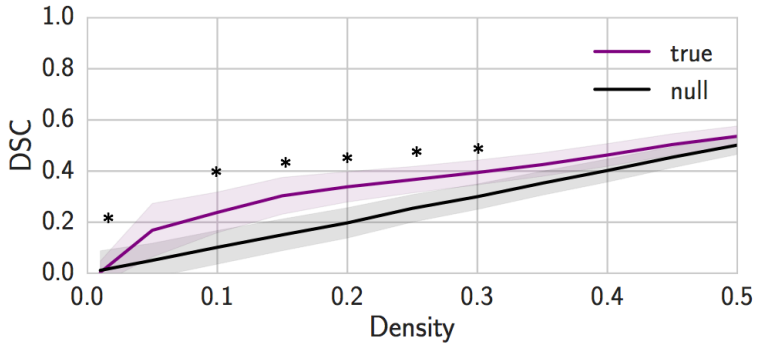


**Supp. Figure 4.3**: Dice Similarity Coefficient (DSC) between functional and structural networks, compared with the DSCs expected from a null distribution. Envelopes represent standard deviations. DSC is significantly greater than chance (*p < 0.05) for most thresholds up to 30%.

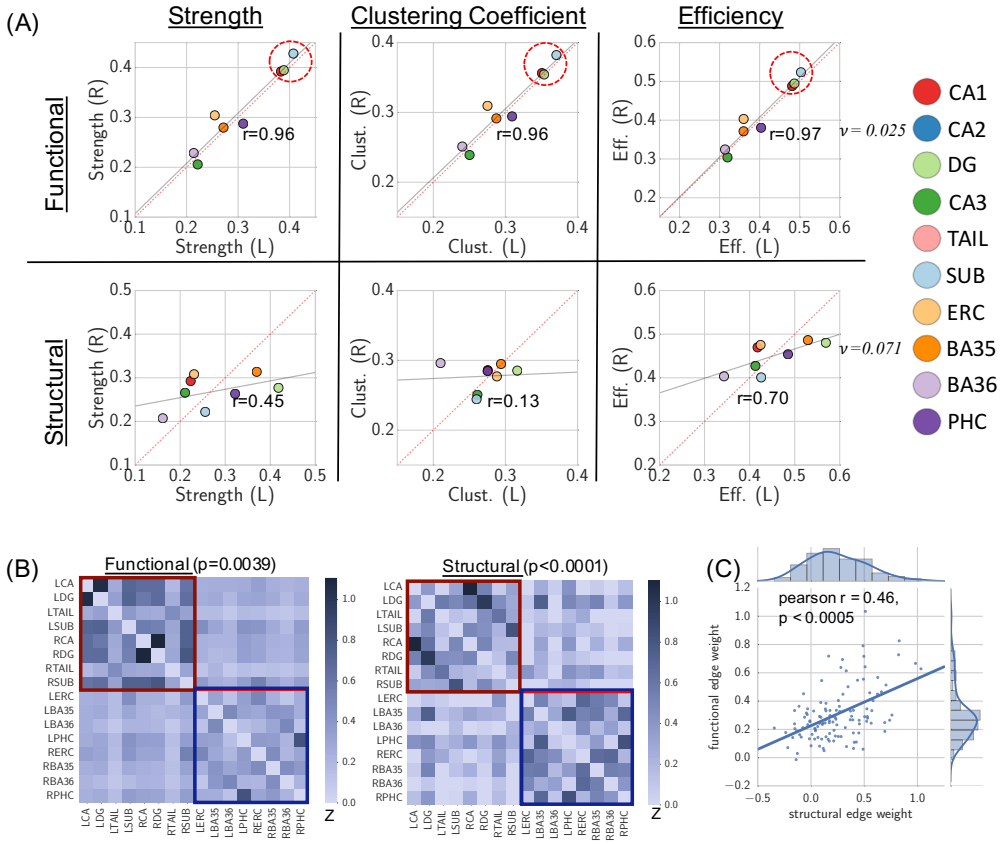


**Supp. Figure 5.1**: Structural and functional analyses replicated after merging CA2/3 subregions with CA1: (A) network symmetry, (B) modular organization, and (C) structure-function correlation. We find significant functional symmetry ($\nu = 0.025$), structural symmetry ($\nu = 0.069$), significant modular organization identical to our original analysis, and significant structure function correlation (r=0.47), revealing that our findings are robust to CA2/3 signal.

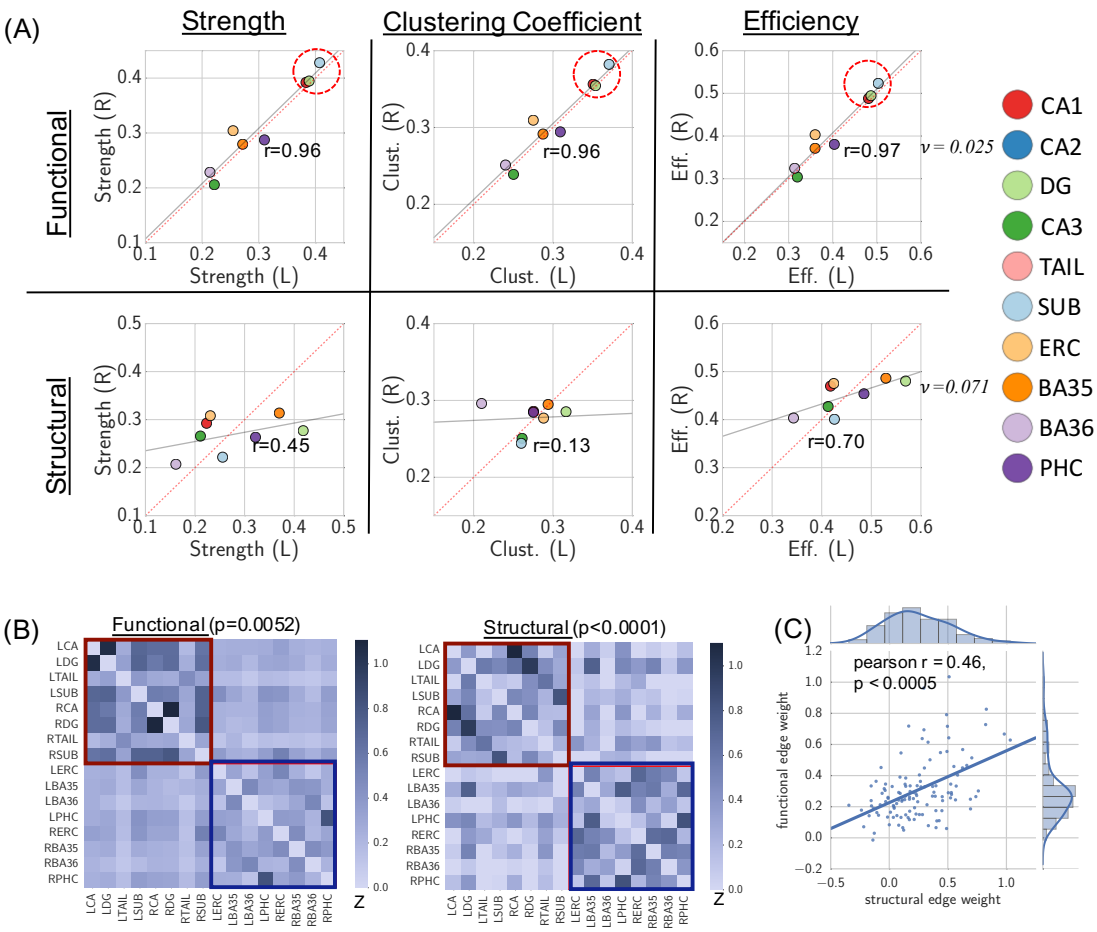


**Supp. Figure 5.2**: Structural and functional analyses replicated after removing CA2/3 subregions: (A) network symmetry, (B) modular organization, and (C) structure-function correlation. We find significant functional symmetry ($\nu = 0.025$), structural symmetry ($\nu = 0.071$), significant modular organization identical to our original analysis, and significant structure function correlation (r=0.46), revealing that our findings are robust to CA2/3 signal.

## S3. Supplemental References:


Harding A, Halliday GM, Kril JJ (1998): Variation in hippocampal neuron number with age and brain volume. *Cereb Cortex* 8:710–718.

Iglesias JE, Augustinack JC, Nguyen K, Player CM, Player A, Wright M, Roy N, Frosch MP, McKee AC, Wald LL, Fischl B, Van Leemput K (2015): A computational atlas of the hippocampal formation using ex vivo, ultra-high resolution MRI: Application to adaptive segmentation of in vivo MRI. *Neuroimage* 115:117–137.

Insausti R, Juottonen K, Soininen H, Insausti a M, Partanen K, Vainio P, Laakso MP, Pitkanen A (1998): MR volumetric analysis of the human entorhinal, perirhinal, and tempropolar cortices. *Am J Med* 19:659–671.

Pruessner JC, Köhler S, Crane J, Pruessner M, Lord C, Byrne A, Kabani N, Collins DL, Evans AC (2002): Volumetry of temporopolar, perirhinal, entorhinal and parahippocampal cortex from high-resolution MR images: considering the variability of the collateral sulcus. *Cereb cortex* 12:1342–1353.

Simic G, Kostovic I, Winblad B, Bogdanovic N (1997): Volume and Number Of Neurons Of the Human Hippocampal Formation In Normal Aging and Alzheimers Disease. *J Comp Neurol* 379:482–494.

Wisse LEM, Kuijf HJ, Honingh AM, Wang H, Pluta JB, Das SR, Wolk DA, Zwanenburg JJM, Yushkevich PA, Geerlings MI (2016): Automated Hippocampal Subfield Segmentation at 7T MRI. *Am J Neuroradiol* 37:1050–1057.